



1 Integrated unmanned aerial vehicle platform with sensing and sampling systems for the
2 measurement of air pollutant concentrations

3 Chen-Wei Liang^{1,2}, Chang-Hung Shen¹

4 ¹ Master Program in UAV Application and Smart Agriculture, National Ilan University, Yilan, Taiwan.

5 ² Department of Biomechatronic Engineering, National Ilan University, Yilan, Taiwan.

6 Correspondence: Chen-Wei Liang (cwliang@niu.edu.tw)

7 Abstract

8 In this study, an unmanned aerial vehicle (UAV) platform with sensing and sampling systems
9 was developed for three-dimensional (3D) measurements of air pollutant concentrations. The sensing
10 system of this platform contains multiple microsensors and Internet of Things devices for determining
11 the 3D distributions of four critical air pollutants and two meteorological parameters in real time.
12 Moreover, the sampling system comprises remote-controllable gas sampling kits, each of which
13 contains a Tedlar bag of 1 L for the 3D measurement of volatile organic compound concentrations
14 according to the TO-15 method of the US Environmental Protection Agency. The performance of the
15 developed UAV platform was verified in experiments where it was used to detect air pollutant
16 emissions from a large industrial zone in Taiwan that included a traditional industrial park, precision
17 machinery park, and municipal waste incineration plant. Three locations were selected as field
18 measurement sites according to the prevailing local wind direction. The vertical distributions of four
19 critical air pollutants, ambient temperature, and relative humidity were determined from data gathered
20 at the aforementioned sites in March and May 2023. A total of 56 and 72 chemical species were
21 qualitatively and quantitatively analyzed in these two periods, respectively. The experimental results
22 verified the feasibility of using the proposed UAV platform for accurately evaluating the air pollutant
23 concentration distribution and transport in an industrial zone. The sampling system can be used as a
24 sampling part of the Method To-15, thus extending the method to measure the 3D distribution of
25 VOCs in an area. The UAV platform can serve as a useful tool in the management and decision-
26 making process of air pollution in industrial areas.

27 **Keywords:** Remote sensing, Low-altitude sampling, EPA method TO-15, Atmospheric monitoring,
28 Vertical profiles, Low-cost microsensors, Particulate matter, Volatile organic compounds

29 1 Introduction

30 Unmanned aerial vehicle (UAV) remote sensing technology has been widely used in a variety of
31 fields, such as defense, agricultural monitoring, surveying and mapping management, and disaster
32 emergency response management (Yang et al., 2022). This technology is also used in environmental
33 monitoring to determine the distributions of pollutants, especially air pollutants (Liu et al., 2020;
34 Zheng et al., 2021; Shen et al., 2022; Sun et al., 2023). UAV systems for air quality monitoring are
35 inexpensive and allow for high-spatiotemporal-resolution data on air pollutant concentrations to be
36 gathered over a large area (Gu et al., 2018). Cozma et al. (2022) proposed an autonomous multirotor
37 aerial platform for the real-time, high-resolution monitoring of air quality in large cities by the



38 obtained fine-grained heat-maps. Duangsuwan et al. (2022) used a UAV system capable of real-time
39 air pollution monitoring and a machine learning method to obtain a three-dimensional (3D) air quality
40 index (AQI) map of an area. Samad et al. (2022) developed a low-cost, practical, and reliable UAV
41 system for the high-resolution 3D profiling of air pollutants at a roadside area. Galle et al. (2021)
42 used a multirotor UAV to obtain in-situ measurements of sulfur dioxide (SO₂), hydrogen sulfide (H₂S),
43 and carbon dioxide (CO₂) concentrations in volcanic gas plumes. De Fazio et al. (2022) developed a
44 remote-controlled UAV with a wide set of sensors to measure the concentrations of air pollutants
45 emitted by waste fires. Samad et al. (2022) developed a UAV system for the 3D profiling of particulate
46 matter (PM), ultrafine particle, and black carbon concentrations. Suroto et al. (2018) designed a
47 waypoint UAV for automatically determining the ambient carbon monoxide (CO) and PM
48 concentrations. Arroyo et al. (2022) developed an electrochemical gas sensing module for a UAV to
49 measure ambient CO, ozone (O₃), nitrogen monoxide (NO), and nitrogen dioxide (NO₂)
50 concentrations. Yungaicela-Naula et al. (2017) used a UAV system and metaheuristic algorithms to
51 measure air pollutant concentrations and track pollution sources in real time. Huang et al. (2022)
52 integrated a UAV platform with an X-ray fluorescence analyzer to develop a high-efficiency system
53 for the rapid detection of heavy metal pollution in soil.

54 UAV remote sensing technology has also been widely used in industrial safety management and
55 agricultural production. Qiu et al. (2017) used a UAV-based monitoring platform and an artificial
56 neural network model to conduct atmospheric dispersion simulation for identifying contaminant
57 sources in a chemical industry park. Xie et al. (2013) proposed a design framework for an emergency
58 atmospheric monitoring system based on a UAV platform. Their platform has high efficiency, high
59 flexibility, and a wide monitoring range. Alvarado et al. (2015) developed a low-cost airborne sensing
60 system based on a UAV platform for monitoring dust particles after blasting at open-pit mine sites.
61 Rotorcraft UAVs are often used to spray pesticides, and the crop movement caused by the rotor of a
62 UAV is a crucial indicator of the effectiveness of the spraying (2023). Boursianis et al. (2022)
63 analyzed the roles of UAV and Internet of Things (IoT) technologies in irrigation, fertilizer application,
64 pesticide application, weed management, plant growth monitoring, crop disease management, and
65 field-level phenotyping. Their results indicated that UAV and IoT technologies are two of the most
66 important technologies for transforming traditional farming practices into precision agriculture
67 practices. Singh and Sharma (2022) proposed a platform for managing the agricultural crop
68 information collected by a UAV, which has high potential for use in agricultural applications such as
69 crop health monitoring, fertilizer spraying, and pesticide spraying.

70 Most UAV environmental monitoring systems used in previous studies have contained various
71 microsensors for measuring air pollutant concentrations. Few studies have proposed designs of UAV-
72 based atmospheric sampling systems for the qualitative and quantitative analysis of low-altitude gas
73 samples. The components of atmospheric gas samples, especially volatile organic compounds
74 (VOC's), can be accurately identified and quantified through a combination of atmospheric sampling
75 and laboratory analysis. In the present study, a UAV platform with sensing and sampling systems was
76 developed for the measurement of low-altitude air pollutant concentrations. The developed UAV

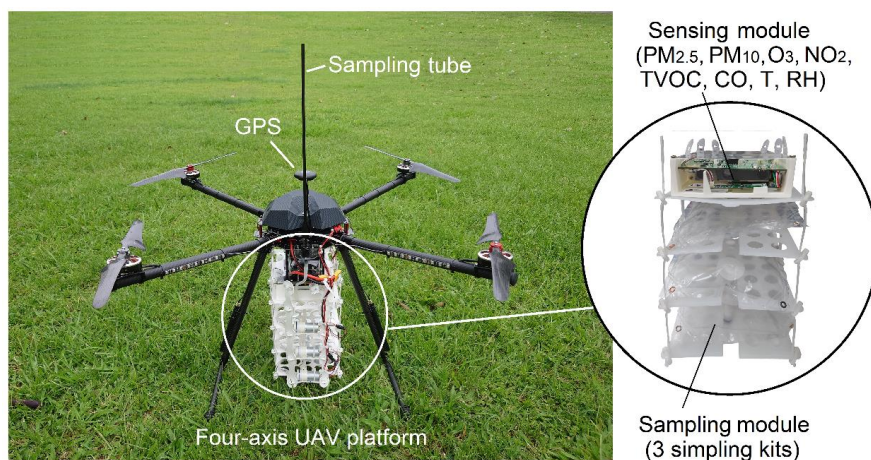


77 platform contains an atmospheric sensing system with various low-cost microsensors for the in-situ
78 measurements of meteorological parameters and air pollutant concentrations to obtain their vertical
79 profiles. Moreover, this platform contains a gas sampling system with multiple remote-controllable
80 gas sampling sets. The gas samples collected by the gas sampling system were analyzed in a
81 laboratory through gas chromatography–mass spectrometry (GC–MS) by using thermal adsorption
82 equipment in accordance with the TO-15 method of the US Environmental Protection Agency (EPA).
83 Finally, the developed UAV platform was verified in field experiments where it collected
84 measurements in a large industrial zone, which included two industrial parks and a municipal waste
85 incineration plant; these measurements were used to determine pollution levels and contamination
86 sources.

87 2 Materials and methodology

88 2.1 Developed UAV platform

89 Figure 1 shows the prototype of the developed UAV platform, which comprises three parts: a
90 UAV, sensing system, and sampling system. The hardware of the platform was constructed using off-
91 the-shelf consumer parts, and the open-source software Ardupilot was used for flight control and data
92 fusion. An all-in-one drone remote control solution for long-range, high-definition video transmission,
93 namely Skydroid H16, was used as the UAV's remote controller. The Pixhawk 6C Flight Controller
94 was used as the autopilot, and the NEO V2 GPS module was used as the unmanned system positioning
95 and navigation module because of its high sensitivity and strong resistance to interference. This
96 module allows for an exact 3D spatial location of the sampling site to better describe the air quality
97 of large spaces.



98
99

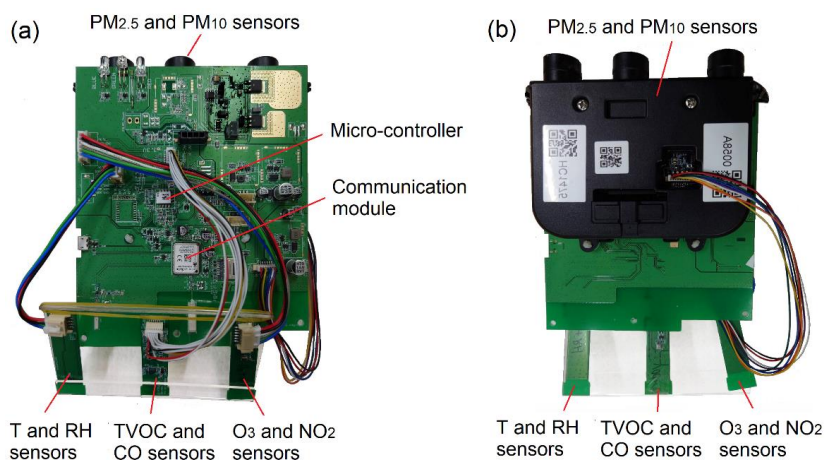
Figure 1. Prototype of the UAV-based air sensing and air sampling systems.

100 2.2 Sensing system

101 The use of low-cost microsensors in a UAV platform offers numerous advantages for the
102 measurement, especially real-time measurement, of the spatiotemporal distribution of air pollutant
103 concentrations (Gu and Jia, 2019; Pochwała et al., 2020). In the present study, a low-cost air quality



104 monitoring kit (Air Quality Detector II, VISION) was used as sensing system in the developed UAV
 105 platform. This monitoring kit is one of the air quality monitor sensors recommended by the Taiwanese
 106 Environmental Protection Administration. The parameters monitored with the aforementioned kit
 107 include PM_{2.5} concentration, PM₁₀ concentration, total VOC (TVOC) concentration, O₃ concentration,
 108 CO concentration, ambient temperature (T) and relative humidity (RH). The sensing system of the
 109 developed UAV platform is connected to an IoT system and a cloud server through a communication
 110 module to track air pollutant concentrations and weather data in real time. The data obtained by the
 111 microsensors of the sensing system are processed by a microprocessor, and the processed data are
 112 transferred to a cloud server for storage through Wi-Fi. The data stored on the cloud server can be
 113 presented in a graphical form in real time. The specifications of the sensing system are listed in Table
 114 1.



115
 116 **Figure 2.** Circuit board with particulate matter and gas sensors used in the UAV platform. (a) front
 117 and (b) back of the circuit board.

118 **Table 1.** Specifications of sensing module

Sensors/devices	Measurement technique/principle	Label/model	Measurement range
T, °C	Bead thermistor	AMS/ENS210	-40 ~ +125
RH, %	Capacitive	AMS/ENS210	0 ~ 100
PM _{2.5} /PM ₁₀ , µg/m ³	Light scattering	VISION/AQ1001	1 ~ 1000
TVOC, ppb	Micro-hot plate technology	AMS/CCS811	0 ~ 29,206
O ₃ , ppb	Metal oxide chemiresistor	Renesas/ZMOD4510	20 ~ 500
NO ₂ , ppb	Metal oxide chemiresistor	Renesas/ZMOD4510	20 ~ 500
CO, ppm	Metal oxide chemiresistor	SGX/MiCS-5524	0.3 ~ 200
Communication module	–	Telit/ME310G1-WW	–
Micro-controller	–	Nuvoton/M481LIDAE	–

119 Prior to each field measurement run, the PM_{2.5}, PM₁₀, O₃, NO₂, TVOC, CO, T, and RH sensors
 120 had to be calibrated using monitoring data from the Wenshan Air Quality Monitoring Station of the



121 Taichung City Environmental Protection Bureau (this station is located in the study area; Fig. 3).

122 2.3 Sampling system

123 The sampling module contains three gas sampling kits that each comprise three mini air pumps
124 (TCS Electrical Co. JQC24381), a 1-L Tedlar bag (Keika Ventures), and a plastic one-way check
125 valve (AliExpress, hose size: 4 mm). The three air pumps of the sampling kits are connected in
126 parallel to a length of 60-cm vertical sampling tube at the top of the UAV. The sampling kits are
127 powered by the batteries of the UAV platform and are individually controlled by the UAV's remote
128 controller. Therefore, the sampling system can perform multipoint sampling at different altitudes or
129 locations in a single flight mission. Multipoint sampling in a single flight can overcome the problem
130 caused by rapidly changing wind fields and makes it easier for representative samples to be obtained.

131 2.4 Analysis of high-altitude VOC concentrations

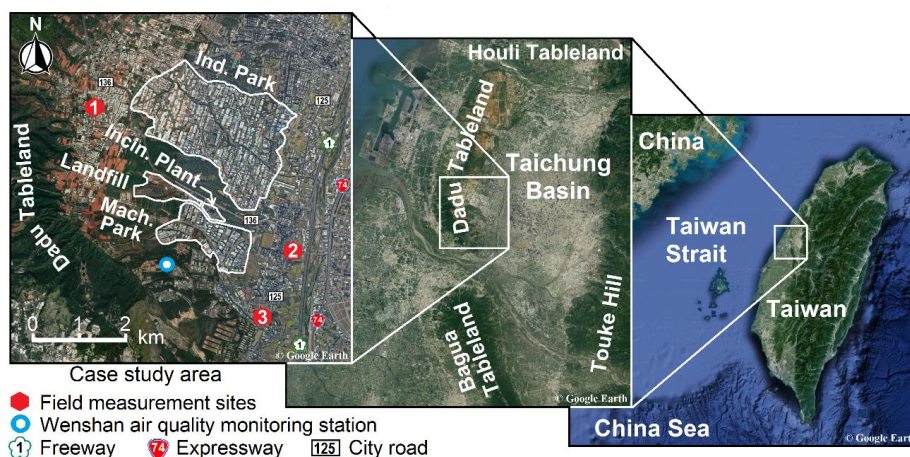
132 The collected gas samples were analyzed in a laboratory in accordance with the TO-15 method
133 of the US EPA. This method is based on criteria for the sampling and analysis of VOC in air and is
134 primarily employed for the monitoring of airborne pollutants in urban and industrial environments.
135 In the TO-15 method, air samples are collected in a special canister. Stainless-steel canisters are too
136 heavy and bulky and thus are unsuitable for use in the developed UAV platform. Therefore, a 1-L
137 Tedlar bag is used instead of a stainless-steel canister in the developed UAV platform. Ambient VOC's
138 were collected in a 1-L Tedlar bag and analyzed by using GC-MS (Shimadzu QP-2010 SE GCMS)
139 and thermal adsorption equipment (ENTECH 7100A Preconcentrator) in accordance with the
140 analytical procedure of the TO-15 method. The analysis column in GC/MS was a Chrompack DB-1
141 capillary column with an inner diameter of 0.25 mm and a length of 60 m. In quantification of VOC
142 species, 101 standard curves were prepared using the standard gases adopted in the calibration
143 mixture of the TO-14A method of the US EPA, the ozone precursor mixtures adopted in the TO-15
144 method. Because these standard curves did not encompass all the compounds in the air samples, a
145 semiquantitative method of analysis was used in which the analyte quantity was based on the standard
146 curve of toluene (in the unit of parts per billion of toluene). Finally, all VOC concentrations were
147 converted to the unit of parts per billion of carbon (ppbC). Because Tedlar bags are not as suitable as
148 canisters for storing samples over long periods (more than approximately 30 days), the collected
149 samples were analyzed within 10 days after sampling.

150 2.5 Field measurements

151 We used the developed UAV platform for detecting air pollutant concentrations in a large special
152 industrial zone that included a traditional industrial park, precision machinery park, and municipal
153 waste incineration plant. Figure 3 shows the location of the study area, which is located at the southern
154 piedmont of the Dadu Tableland in the western part of the Taichung Basin, Taiwan. Two industrial
155 parks [Taichung Industrial Park (TIP) and Taichung Precision Machinery Park (TPMP)], a municipal
156 waste incineration plant [Wenshan Waste Incineration Plant (WWIP)], and a landfill (Wenshan
157 Landfill) were located within the study area. The TIP is a large industrial space with a total area of
158 5.82 km². Currently, 1086 factories that employ a total of approximately 44 000 people are located in



159 this industrial park. In addition to traditional industries, high-tech industries, such as optoelectronics,
160 electronics, and precision machinery industries, are located in TIP. TPMP is an industrial park with
161 an area of 1.61 km² and mainly includes companies focusing on precision machinery innovation. This
162 industrial park is a crucial base of production of Taiwan's machinery industry and has a land sales
163 rate of 100%. As of the end of December 2022, 170 manufacturers that employ approximately 21 329
164 people operate in TPMP. WWIP began operation in 1995 and was the first large-scale incineration
165 plant to be established in central Taiwan. This plant covers an area of 0.044 km² and has three
166 incinerators that handle a total of 900 tons of waste per day. Wenshan Landfill was opened in 1983
167 and covers an area of 0.365 km². The restoration of this landfill was completed in March 2019 and
168 involved the installation of a solar photovoltaic system with a capacity of approximately 6.2 MWp
169 on an area covering 0.0483 km². In addition, a busy national freeway and provincial expressway were
170 located in the eastern part of the study area (Fig. 3) with weekday southbound and northbound traffic
171 volumes of approximately 112 150 and 85 480 PCU, respectively.

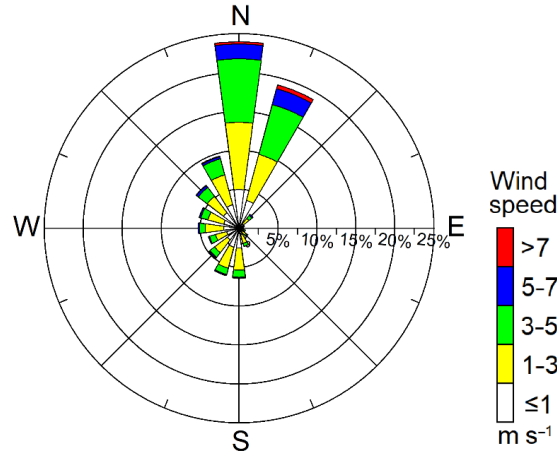


172
173 **Figure 3.** Locations of field measurement sites and Wenshan air quality monitoring station in the
174 case study area.

175 The annual prevailing wind directions in the study area are north and north–northeast, which can
176 be attributed to the spoon-shaped topography of the Dadu Tableland (Fig. 4). Moreover, the most
177 prevalent local average wind speed is 1–3 m s⁻¹, followed by 3–5 m s⁻¹. Therefore, three locations
178 were selected as field measurement sites (sites 1, 2, and 3) according to the prevailing wind directions
179 (Fig. 4). These sites were located in densely populated parts of the study area. Site 1 was located
180 upwind of the two industrial areas and WWIP, whereas sites 2 and 3 were located downwind of these
181 areas and WWIP. Because of regulations limiting the altitude of local flights to 200 ft (61 m), the
182 heights at which samples were gathered were 2, 20, 40, and 60 m above the ground at each site. Noori
183 and Dahnil (2020) indicated that a UAV monitoring system can accurately measure the concentrations
184 of air pollutants at flight speeds slower than 6 m s⁻¹ and that detection accuracy decreases
185 considerably at flight speeds greater than 8 m s⁻¹. Therefore, the flight speed of the developed UAV



186 platform was controlled at $\leq 6 \text{ m s}^{-1}$ in this study.



187
 188

Figure 4. Annual wind rose of 2022 at the Wenshan air quality monitoring station.

189 2.6 Measurement of the speed and direction of the upper winds

190 To avoid the airflow caused by the rotor of the UAV from affecting the measurement of the speed
 191 and direction of the upper winds, the single-theodolite method was used in this study. A theodolite
 192 (WORLD E105-S Theodolite) was used to measure the speed and direction of the upper winds
 193 according to the pilot-balloon observation method (Pollak and Brunt, 1939). Figure 5 shows a
 194 schematic of the measurement of the upper winds by using the single-theodolite method, with Figs.
 195 5(a) and 5(b) displaying the ground-projection-based and sliding-rule-based wind field diagrams,
 196 respectively. The formula for computing the speed of the upper winds is as follows:

197
$$u = 72L^{0.63} / (L + W)^{0.42} \quad (1)$$

198
$$r_1 = Z_1 \cot H_1 \quad (2)$$

199
$$V_e = Z_2 \cot H_2 \sin A_2 - Z_1 \cot H_1 \sin A_1 \quad (3)$$

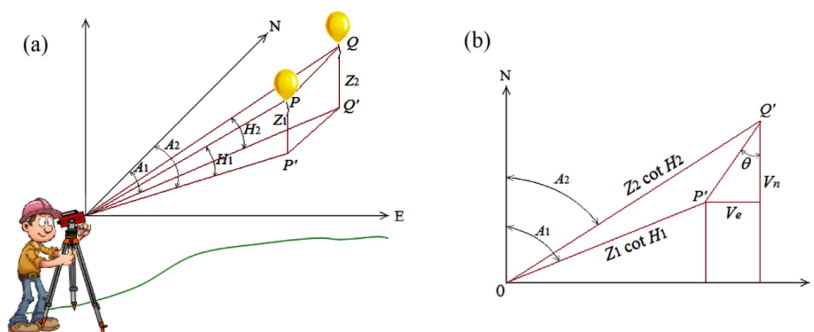
200
$$V_n = Z_2 \cot H_2 \cos A_2 - Z_1 \cot H_1 \cos A_1 \quad (4)$$

201
$$\theta = \tan^{-1}(V_e/V_n) \quad (5)$$

202
$$P'Q' = V_e / \sin \theta \quad (6)$$

203
$$V = P'Q' / t \quad (7)$$

204 where u , L , and W are the rising speed (m/s), buoyancy (g), and weight of the pilot balloon (g),
 205 respectively; r_1 , Z_1 , and H_1 are the projected length (m) from the ground up to point p , the rising
 206 height (m), and the elevation angle ($^\circ$), respectively; V_e and V_n are the eastern and northern projection
 207 lengths (m) of the wind speed, respectively; θ , A_i , and V are the northeastern wind speed angle ($^\circ$),
 208 azimuth angle ($^\circ$), and average wind speed at time t , respectively; and $P'Q'$ is PQ at ground projection
 209 (m). The wind directions at $P'Q'$ in quadrants I, II, III, and IV are defined to be $180^\circ + \theta$, $180^\circ - \theta$, θ ,
 210 and $360^\circ - \theta$, respectively.



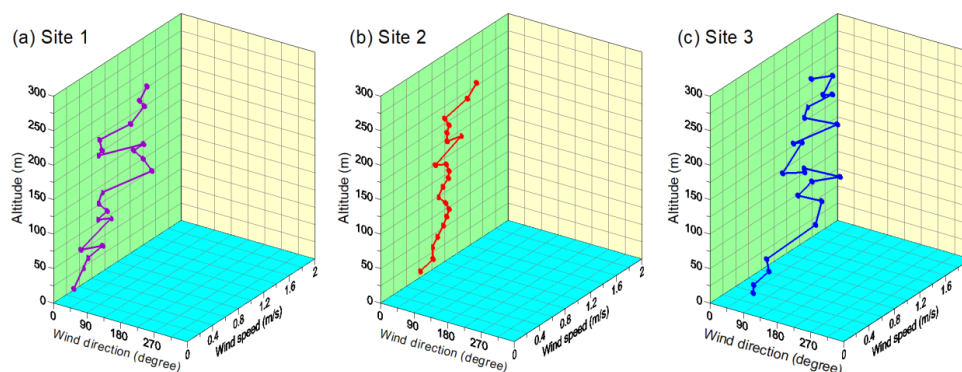
211
 212 **Figure 5.** (a) geometry of the single-theodolite method and (b) the slide-rule method of computation.

213 **3 Results and discussion**

214 3.1 Field measurement 1

215 3.1.1 Upper winds

216 Figure 6 illustrates the observation results for the upper winds at the three field measurement
 217 sites between 13:30 and 16:30 on 29 March 2023. During the observation period, all wind directions
 218 at the three sites were between the north and northeast. All upper wind speeds observed at the three
 219 sites were less than 2 m s^{-1} . The prevailing wind directions at sites 1, 2, and 3 were north–northeast,
 220 north by east, and northeast, respectively. The wind speed at site 3 on the southern (downwind) side
 221 was marginally higher than those at the other two sites. The wind speeds at the three sites increased
 222 with altitude, which is consistent with the power law of the vertical distribution of wind speed. In the
 223 Taichung Basin, the average hourly wind speed was mostly between 0 and 3 m s^{-1} . The sampling
 224 period coincided with a period of comfortable weather in Taiwan.



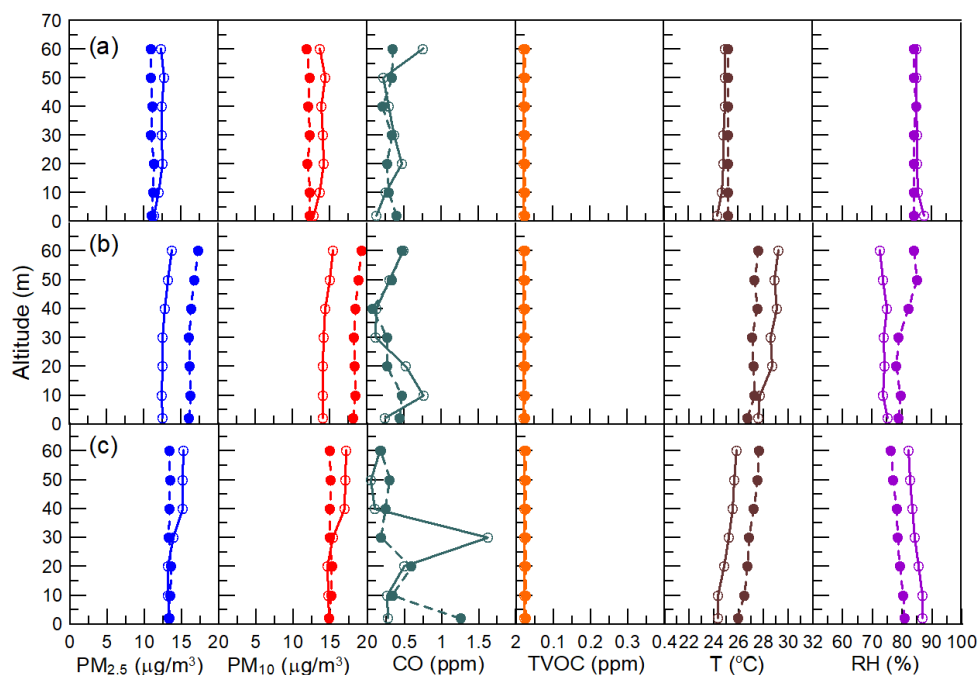
225
 226 **Figure 6.** The observation results of upper winds during 13:30–16:30 on 29 March 2023, (a)–(c) are
 227 at sites 1–3, respectively.

228 3.1.2 Vertical distributions of critical air pollutants

229 Prior to each UAV telemetry run, the sensing system was connected to the IoT system to ensure
 230 that the monitoring data were input to the cloud server. Two runs were conducted at each monitoring
 231 site; thus, six runs were performed in total. Figure 7 displays the vertical distributions of critical air



232 pollutants, ambient temperature, and RH during 13:30–16:30 on 29 March 2023. In Fig. 7, the solid
 233 and dashed lines represent the results obtained in runs 1 and 2 at each site, respectively. The PM_{2.5}
 234 and PM₁₀ concentrations at the three sites were 11.0–17.3 (average = 13.4) and 11.9–19.3 (average =
 235 15.0), respectively. The highest and lowest concentrations of PM (both PM_{2.5} and PM₁₀) were
 236 observed at sites 2 (downwind) and 1 (upwind), respectively. The results indicate that the investigated
 237 industrial zone had high local PM concentrations, especially at site 2. CO is mainly emitted from
 238 mobile sources. Although the CO concentrations at the three sites were marginally variable but low.
 239 Therefore, the differences in the influences of the mobile source on the three locations were small.
 240 The TVOC concentrations at the three sites were very low (≤ 0.02 ppm), which might be attributable
 241 to the lack of large VOC emission sources in the investigated industrial zone. Because the sensitivities
 242 of the O₃ and NO₂ sensors were too low (Table 1), their monitoring data were 0 ppm in all the
 243 measurements.



244

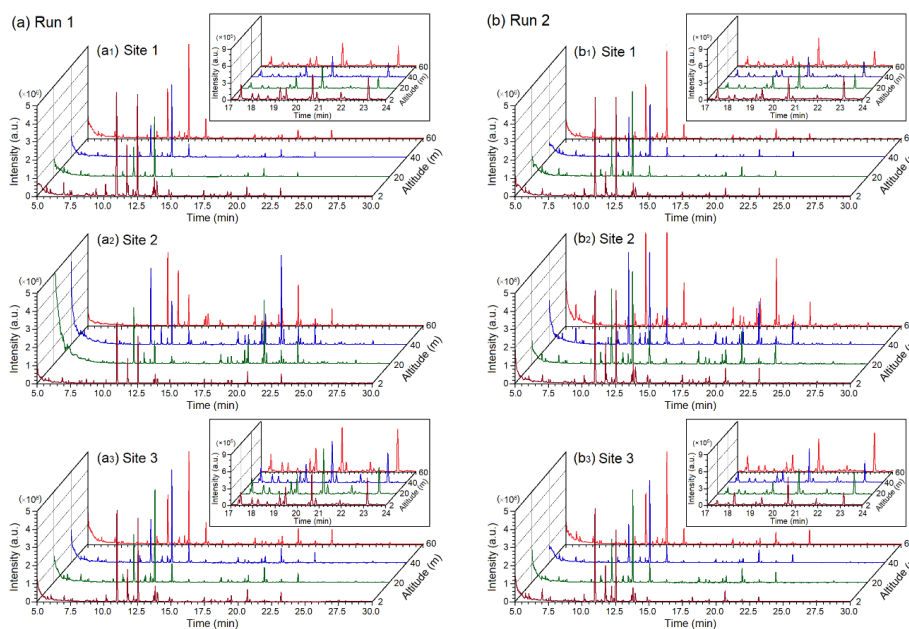
245 **Figure 7.** The observation results of critical air pollutants, ambient temperature, and relative humidity
 246 during 13:30–16:30 on 29 March 2023, (a)–(c) are at Sites 1–3, respectively. Solid and dashed lines
 247 are the results of Run 1 and Run 2, respectively.

248 The temperature ranges at sites 1 to 3 were 24.3–25.2 °C (average = 25.0 °C), 26.7–29.2 °C
 249 (average = 27.9 °C), and 24.3–27.6 °C (average = 26.0 °C). At all locations, the lowest temperature
 250 was observed at the ground because of the heat radiation from the surface on cloudy days. The
 251 temperatures at the three sites gradually decreased in the afternoon with time. The RH values of the
 252 three locations changed with the temperature, and the RH range in the study area was 76.1%–87.6%.



253 3.2.3 Vertical distributions of VOCs

254 Sampling was performed twice at four altitudes at each site by using the UAV platform; thus,
255 eight samples were collected per site. Figure 8 displays the analysis results obtained through GC–MS
256 with thermal adsorption equipment for the upper-altitude VOCs at the three sites during 13:30–16:30
257 on 29 March 2023, using GC–MS. A total numbers more than 56 species were analyzed at different
258 altitudes at the each site. The analysis results indicated the feasibility of using the developed UAV
259 platform with Tedlar bag sampling system for the 3D measurement of VOC concentrations in
260 accordance with the TO-15 method. All dominant VOCs at various altitudes at the three sites appeared
261 within the retention time of 10–15 min in GC-MS chromatography. The peak patterns of the dominant
262 species at the three sites were highly similar, which indicated that the three sites had similar air
263 pollution sources. A second set of dominant VOCs appeared at various altitudes within the retention
264 time of 17–24 min, especially at site 3. The second dominant species at site 2 had a considerably
265 higher concentration than did those at the other sites, which indicated that site 2 was located
266 downwind of some air-pollution emission sources. TIP is located upwind of site 2 (Fig. 3).



267

268 Fig. 8. The analysis results of upper-altitude VOCs during 13:30–16:30 on 29 March 2023. (a) and
269 (b) show the results of run 1 and run 2, respectively. The insets in each subfigure are zoomed-in views
270 over the retention time range from 17 to 24 minutes.

271 Table 2 lists the qualitative and quantitative analysis results of the VOC samples collected from
272 the three sites, where the concentration is the average of those obtained in two sampling runs (runs 1
273 and 2 in Fig. 8). The concentrations of the top five VOC species at the four sampled altitudes had the
274 following order from highest to lowest: site 1, toluene > 2,4-dimethyl heptane > 4-methyl octane >
275 propyl propionate > 3,7-dimethyl undecane; site 2, 2,4-dimethyl heptane > toluene > 4-methyl octane



276 > 3,7-dimethyl undecane > propyl propionate; and site 3, 2,4-dimethyl heptane > toluene > 4-methyl
 277 octane > propyl propionate > 3,7-dimethyl undecane. The ranges of the concentration ratio of the top
 278 five species to all upper-altitude VOCs at sites 1, 2, and 3 were 71.1%–80.9% (average = 74.9%),
 279 69.1%–79.7% (average = 72.9%), and 72.3%–76.8% (average = 73.6%), respectively. Thus, the top
 280 five VOC species dominated the upper-altitude VOC concentrations.

281 **Table 2.** The average concentrations (in ppbC) of upper-altitude VOCs at the three sites during March 29, 2023.

Species	Retention time (min)	Altitude at Site 1 (m)				Altitude at Site 2 (m)				Altitude at Site 3 (m)			
		2	20	40	60	2	20	40	60	2	20	40	60
Ethanol	5.70	1.8	2.3	1.4	1.2	0.6	2.9		5.1	1.7	1.2	1.7	2.0
Acetone	5.98	0.8	0.8	0.8	0.6	0.9	0.8	1.4	1.2	1.4	1.2	0.8	0.9
Isopropanol	6.11	0.6	0.9						0.6				
2-Methyl pentane	6.99	3.9	3.5	2.6	3.0	3.3	4.7	9.0	4.8	5.1	4.4	2.7	3.6
2-Butanone	7.29	0.3	0.3	0.3	0.3	0.2	0.2	0.3	0.2	0.3	0.3	0.3	0.3
Hexane	7.48	1.4	0.6	0.6	0.6	1.4	1.1	1.2	0.9	0.8	0.9	0.6	1.2
Ethyl Acetate	7.58	1.1	0.8	0.8	0.8	0.8	0.9	0.8	0.9	1.1	0.8	0.8	0.8
Benzene	8.59		0.2	0.2	0.2	0.5	0.8	0.9	1.1	0.3	0.5	0.5	0.3
1-Butanol	8.62	0.5			0.2					0.2			
2-Methyl hexane	8.73	0.3	0.5	0.3	0.2		0.3	0.5	0.5	0.2	0.3	0.3	0.3
Cyclohexane	8.91	0.5											
3-Methyl hexane	8.95	0.3	0.2	0.2	0.2	0.3	0.3	0.5	0.5	0.5		0.3	0.3
Pentanal	9.07	0.2	0.0	0.0	0.0					0.2		0.0	0.2
1,2-Dichloro propane	9.19	1.2				0.5				0.8			
Heptane	9.40	1.7	1.1	0.9	1.1	1.8	1.8	2.6	2.0	1.2	1.2	1.1	1.2
2,5-Dimethyl hexane	10.12	3.5	2.1	1.7	2.4	2.7	4.2	5.0	4.4	2.4	2.7	2.3	2.7
2,4-Dimethyl hexane	10.19	0.8	0.5	0.5	0.8	0.8	1.1	1.4	1.4	0.8	0.8	0.6	0.8
2,5-Dimethyl-1-hexene	10.58	0.2	0.0	0.0	0.0			0.2	0.0	0.0	0.0	0.0	0.0
2-Ethyl-1-butanol	10.70	0.5	0.3	0.3	0.5		0.5	0.5	0.5	0.3	0.5	0.3	0.5
Toluene	10.94	87.9	16.5	17.3	25.1	71.3	35.7	45.5	45.2	49.2	23.0	19.7	24.5
3-Methyl heptane	11.15	0.3	0.2	0.2	0.2		0.5	0.3	0.3	0.3	0.2	0.2	0.3
Hexanal	11.44	0.5	0.3	0.3	0.5	0.5	0.5	0.5	0.6	0.5	0.5	0.5	0.5
Propyl propionate	11.71	15.6	0.3	0.3	0.9	17.1	1.2	1.5	2.3	13.7	0.6	0.5	0.9
Octane	11.79	3.5	1.8	1.4	2.0	2.1	3.5	3.5	3.9	1.1	2.0	1.7	2.1
2,3,5-Trimethyl hexane	12.36	1.2	0.8	0.8	0.9	1.2	1.7	2.0	2.3	1.1	1.4	1.1	1.1
2,4-Dimethyl heptane	12.50	42.9	28.1	24.6	41.3	43.8	62.4	77.4	81.6	30.5	38.6	35.3	42.2
2,6-Dimethyl heptane	12.66	0.3	0.2	0.2	0.2	0.3		0.3	0.5		0.2	0.2	0.2
2,4-Dimethyl-1-heptene	13.06	0.2	0.2	0.2	0.2	0.3	0.3	0.3	0.3	0.2	0.2	0.2	0.2
3-Ethyl-2-methyl hexane	13.60	0.2	0.0	0.2	0.2		0.5	0.5	0.6	0.2	0.3	0.3	0.3
Ethyl benzene	13.68	3.0	0.0	0.2	0.2	3.9				2.4		0.3	0.3
4-Methyl octane	13.77	6.5	3.8	4.7	6.9	7.8	13.4	15.6	17.7	5.7	6.9	6.9	8.0
m-Xylene	13.94	10.4	0.5	0.6	1.2	14.7	2.3	2.1	2.9	7.8	0.9	1.2	1.5
o-Xylene	14.84	3.3		0.3	0.6	6.6	0.9	0.9	1.4	3.5	0.6	0.5	0.3
Nonane	15.03	1.1	0.5	0.6	0.8	1.5	2.0	2.7	3.2	0.8	1.1	1.1	1.2
2,4,6-trimethyl heptane	15.80							0.2	0.3				0.2
3,5-Dimethyl octane	16.04	0.2		0.0	0.2		0.3	0.3	0.5		0.2		0.2
2,7-Dimethyl octane	16.18	0.3	0.2	0.2	0.3	0.8	1.1	1.2	1.4	0.5	0.5	0.5	0.5
2,6-Dimethyl octane	16.40	0.2					0.3	0.5	0.5		0.2		0.2
2,5-Dimethyl octane	17.36	0.3	0.2	0.2	0.3	0.6	1.2	1.1	1.7	0.3	0.3	0.3	0.5
2-Methyl nonane	17.44	1.5	0.6	0.8	1.2	2.4	4.2	3.9	5.9	0.9	1.2	1.4	1.8
2,5-Dimethyl nonane	17.95	0.6	0.5	0.5	0.6	1.2	2.4	2.6	3.8	0.6	0.9	0.9	0.9
Decane	18.64	0.3	0.2	0.2	0.3	0.6	1.1	0.9	1.4	0.3	0.3	0.3	0.5
4-Methyl decane	19.07	0.2	0.2	0.2	0.2	0.2	0.5	0.8	1.2	0.2	0.2	0.2	0.2
Undecane	19.20	0.9	0.5	0.6	0.8	1.7	3.2	3.0	5.7	0.8	0.9	1.1	1.2
2,5,6-Trimethyl decane	19.36	0.3	0.2	0.2	0.2	0.3	0.9	0.8	1.5	0.3	0.3	0.3	0.3
4-Methyl-5-propyl nonane	19.47	1.1	1.1	0.8	0.9	1.8	3.9	4.7	7.5	1.2	1.5	1.4	2.0
Dodecane	20.53	0.3	0.2	0.2	0.2	0.3	0.8	1.2	1.7	0.3	0.3	0.3	0.5
3,7-Dimethyl undecane	20.65	2.4	2.6	2.1	2.6	4.4	9.2	12.8	19.1	3.2	3.5	3.8	3.9
4-Methyl-1-undecene	20.84	0.2	0.0	0.2	0.2	0.2	0.5	0.5	0.9	0.2	0.2	0.2	0.2
Undecanal	21.56			0.2			0.3	0.3	0.5			0.2	0.2
2,3-Dimethyl decane	21.77		0.2	0.2	0.2		0.5	0.6	0.9	0.2	0.2	0.2	0.2
Tridecane	21.93	0.5	0.3	0.2	0.5	0.8	1.5	2.1	2.7	0.5	0.6	0.6	0.8
2,3,5,8-Tetramethyl decane	22.09	0.2	0.0	0.2	0.2		0.5	0.6	0.9	0.2	0.2	0.2	0.2
2-Heptyl-1,3-dioxolane	22.27			1.5	1.5								
2-Methyl tridecane	23.59						0.3	0.5	0.6				0.0
2,6-Dimethyl undecane	24.00						0.2	0.5					
Total		204.8	72.9	69.5	102.3	199.5	176.1	214.8	244.2	143.3	101.7	92.6	111.9

282 Toluene and 2,4-dimethyl heptane exhibited the highest or second-highest concentrations among
 283 the VOCs at the three sites. Toluene might originate from vehicle exhaust and industrial emissions.

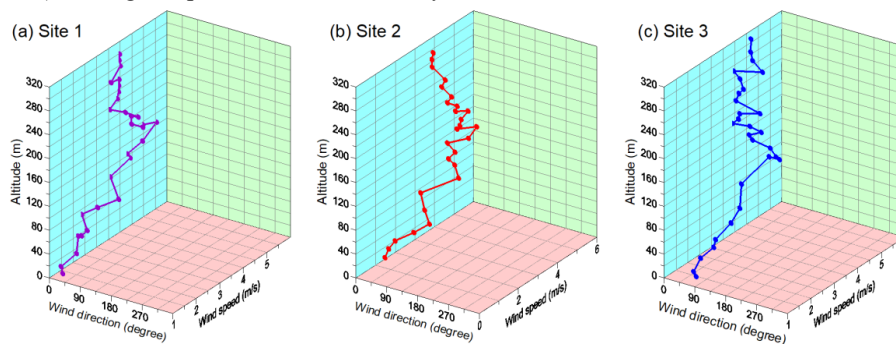


284 Common industrial organic solvents, such as benzene, xylene, ethylbenzene, and butanone, were
285 detected at the four altitudes at each site, which indicated that a considerable quantity of the toluene
286 in the study area originated from industrial emissions. In general, because its branched structure
287 allows for combustion without knocking, 2,4-dimethyl heptane is blended with other gasoline
288 components to produce high-octane fuel. In addition, alkanes were the dominant VOC species at
289 various altitudes and sites. Thus, the concentrations of the VOCs originating from vehicle exhaust
290 might have been higher than those of the VOCs originating from industrial exhaust. Propyl propionate
291 is a safer alternative for toluene because of its low odor, moderately volatile nature, and nonhazardous
292 and nonpolluting ester product; thus, the propyl propionate detected field measurement 1 mainly
293 originated from industrial emissions. The average VOC concentrations at the three sites had the
294 following order from highest to lowest: site 2 > (site 1 \approx site 3). The highest and second-highest total
295 VOC concentrations at sites 1 and 3 appeared at altitudes of 2 and 60 m, respectively. By contrast,
296 the highest and second-highest total VOC concentrations at site 2 appeared at altitudes of 60 and 40
297 m, respectively. This result indicates that some VOCs were transmitted from upwind sources.

298 3.2 Field measurement 2

299 3.2.1 Upper winds

300 Figure 9 shows the observation results for the upper winds at the three field measurement sites
301 between 13:30 and 16:30 on 10 May 2023. During the measurement period, all wind directions at the
302 three sites were between north and east. The prevailing wind directions at sites 1, 2, and 3 were north-
303 northeast, northeast by east, and northeast by east, respectively. The upper wind speeds at sites 1–3
304 were 1.1–5.6 m s⁻¹ (average = 3.5 m s⁻¹), 1.2–5.1 m s⁻¹ (average = 3.6 m s⁻¹), and 1.2–5.2 m s⁻¹
305 (average = 3.7 m s⁻¹), respectively. The wind speeds at the three sites increased with an increase in
306 altitude but decreased marginally as the altitude increased beyond 200 m. Compared with the upper
307 winds during the field measurement 1 (on 29 March 2023), those during field measurement 2 (on 10
308 May 2023) had higher speed and a more easterly direction.



309
310

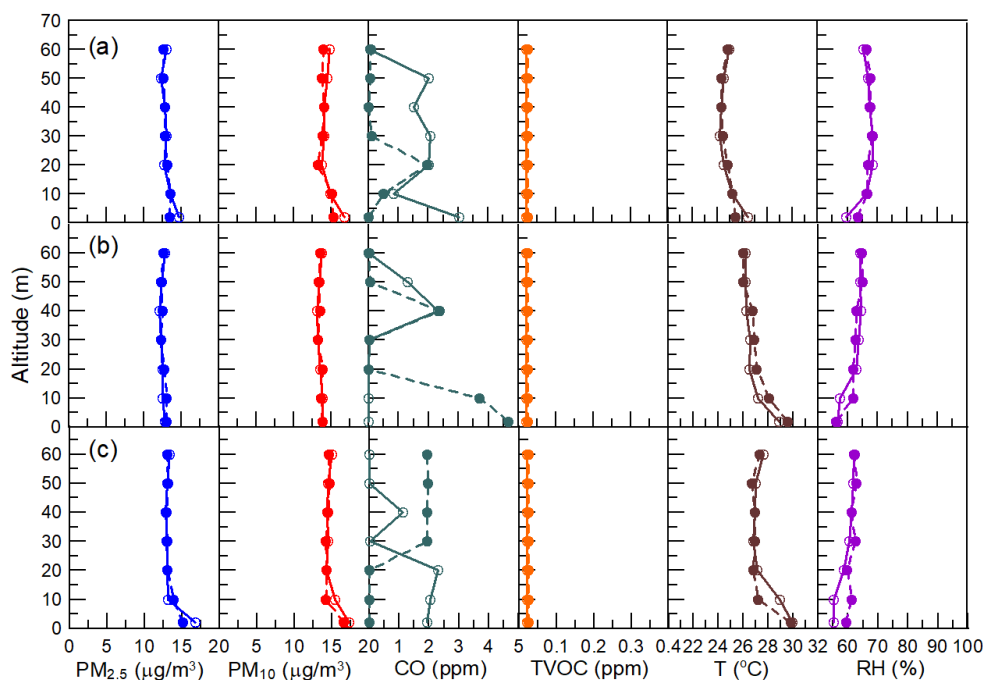
Figure 9. The observation results of upper winds during 13:30–16:30 on 10 May 2023.

311 3.2.2 Vertical distributions of critical air pollutants

312 As was the case in field measurement 1, two runs of UAV telemetry were implemented at each
313 monitoring site; thus, a total of six runs were performed. The sensing system was connected to the



314 IoT system prior to UAV telemetry to ensure that the monitoring data were input to the cloud server
 315 after each run. Figure 10 displays the vertical distributions of critical air pollutants, ambient
 316 temperature, and RH for the period of 13:30–16:30, 10 May 2023. The PM_{2.5} and PM₁₀ concentration
 317 ranges at the three sites were 12.1–16.8 $\mu\text{g m}^{-3}$ (average = 13.1 $\mu\text{g m}^{-3}$) and 13.1–17.4 $\mu\text{g m}^{-3}$
 318 (average = 14.3 $\mu\text{g m}^{-3}$), respectively. The highest and lowest concentrations of PM (both PM_{2.5} and
 319 PM₁₀) were observed at sites 3 (downwind) and 2 (upwind), respectively. The highest CO
 320 concentrations at the three sites was at the ground level, and the highest CO concentration of 4.66
 321 ppm was measured at site 2. The CO concentrations at all altitudes except for the ground level at the
 322 three sites varied between 0 and 2.4 ppm. As was the case in field measurement 1, the O₃ and NO₂
 323 concentrations were 0 ppm in measurement 2 because the sensitivities of the O₃ and NO₂ sensors
 324 were too low. The TVOC concentrations at the three sites were very low (≤ 0.02 ppm; as in field
 325 measurement 1), possibly because the sensitivity of the TVOC sensor was too low.



326

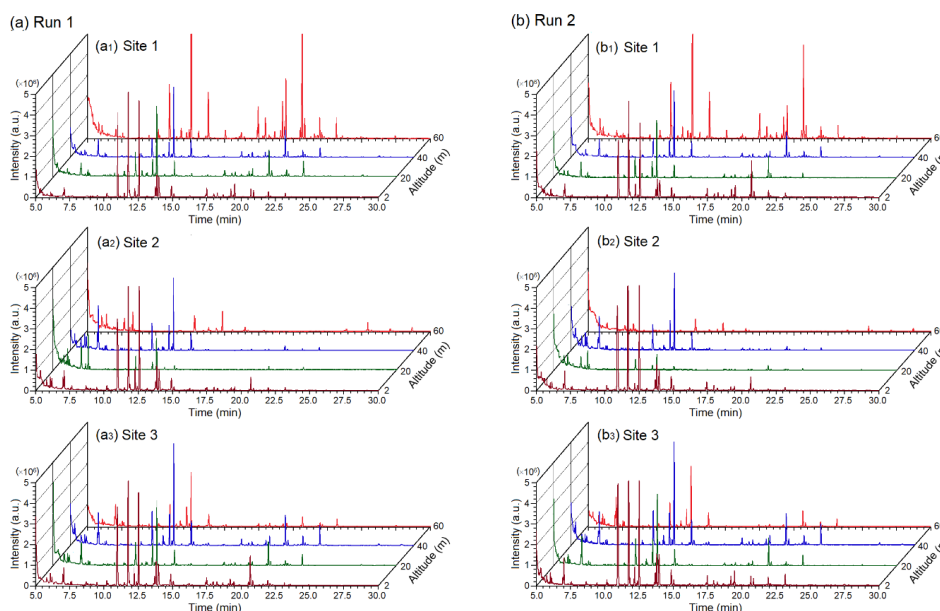
327 **Figure 10.** The observation results of critical air pollutants, ambient temperature, and relative
 328 humidity during 13:30–16:30 on 10 May 2023, (a)–(c) are at sites 1–3, respectively. Solid and dashed
 329 lines are the results of run 1 and run 2, respectively.

330 The temperature ranges at sites 1–3 were 24.12–26.4 $^{\circ}\text{C}$ (average = 24.9 $^{\circ}\text{C}$), 26.0–29.6 $^{\circ}\text{C}$
 331 (average = 27.0 $^{\circ}\text{C}$), and 26.7–29.9 $^{\circ}\text{C}$ (average = 27.6 $^{\circ}\text{C}$), respectively. The highest temperatures at
 332 these sites were observed at the ground level because of the thermal radiation of the surface on sunny
 333 days. The temperatures at the three sites gradually decreased in the afternoon with time. The RH
 334 values of the three sites changed with the temperature, and the RH range in the study area was 55.1%–
 335 68.4%.



336 3.2.3 Vertical distributions of VOCs

337 Figure 11 depicts the GC–MS analysis results for upper-altitude VOCs at the three field
338 measurement sites during 13:30–16:30 on 10 May 2023. Sampling was performed twice at four
339 altitudes (2, 20, 40, and 60 m) at each site by using the UAV platform; thus, a total of 24 measurements
340 were performed (eight at each site). A total of 79 VOCs species were analyzed at different altitudes
341 at the three sites, and this number is higher than the number of VOCs analyzed in field measurement
342 1 (i.e., 52). All the dominant VOC species at various altitudes at the three sites appeared within the
343 retention time of 10–15 min in GC–MS chromatogram, which is line with the results obtained in field
344 measurement 1. The peak patterns of the dominant VOC species at the three sites were highly similar,
345 which indicated that the three sites had similar air pollution sources. The highest peak intensities of
346 the dominant VOC species at the three locations were observed at an altitude of 2 m. A second
347 dominant VOC species appeared at various altitudes within the retention time of 17–24 min,
348 especially at an altitude of 60 m at site 1. The peak intensity of the second dominant species at site 2
349 was considerably lower than those at the other two sites. In addition, the concentrations of all the
350 VOCs at an altitude of 60 m at site 2 were lower than those at the same altitude at sites 1 and 3.



351
352 **Figure 11.** The analysis results of upper-altitude VOCs during 13:30–16:30 on 10 May 2023. (a) and
353 (b) show the results of run 1 and run 2, respectively.

354 Table 3 lists the average upper-altitude VOC concentrations at the three sites on 10 May 2023.
355 The total upper-altitude VOC concentrations at the three sites in field measurement 2 was marginally
356 lower than that in field measurement 1; however, the total number of VOC's detected in field
357 measurement 2 was higher than that in field measurement 1. In addition, the highest and lowest VOC
358 concentrations occurred at an altitude of 2 m at site 3 and at an altitude of 60 m at site 1, respectively.
359 This result is different to that obtained in field measurement 1.



361 The top five VOCs at the four altitudes had the following order from highest to lowest: site 1,
362 2,4-dimethyl heptane > toluene > propyl propionate > 3,7-dimethyl undecane > tetramethylsilane;
363 site 2, propyl propionate > 2,4-dimethyl heptane > toluene > 2-methyl pentane >
364 hexamethylcyclotrisiloxane; and site 3, 2,4-dimethyl heptane > toluene > propyl propionate > 2-
365 methyl pentane > tetramethylsilane. The ranges of the concentration ratios of the top five species to
366 all the upper-altitude VOCs at sites 1, 2, and 3 were 56.0%–68.5% (average = 61.5%), 51.7%–72.6%
367 (average = 60.1%), and 54.1%–67.9% (average = 59.5%), respectively. The predominance of the top
368 five species in the total upper-altitude VOC concentration in field measurement 2 was lower than that
369 in field measurement 1, which was because more VOCs were detected in field measurement 2 than
370 in field measurement 1.

371 2,4-Dimethyl heptane and toluene had the highest and second-highest concentrations among the
372 VOCs at sites 1 and 3, respectively. However, at site 2, they had the second- and third-highest
373 concentrations, respectively, with propyl propionate having the highest concentration. Toluene is the
374 most common organic compound and originates from vehicle exhaust and industrial emissions. At
375 each site, the detected concentrations of industrial organic solvents, such as benzene, xylene,
376 ethylbenzene, butanone, acetone, isopropyl alcohol, and ethyl acetate, were higher in field
377 measurement 2 than in field measurement 1. Isopropyl alcohol is a crucial cleaning agent and
378 disinfectant in high-tech factories. The second largest high-tech park in Taiwan is located
379 approximately 4 km north of the study area. Thus, a considerable quantity of the toluene detected in
380 field measurement 2 originated from industrial emissions. 2,4-Dimethylheptane is a crucial
381 component of high-octane fuel, such as gasoline; thus, the detected 2,4-dimethylheptane content
382 mainly originated from vehicle emissions. Hexamethylcyclotrisiloxane is used as an additive in the
383 creation of plastic and rubber products, paints, adhesives, cosmetics, food packaging, and many other
384 products; thus, the detected hexamethylcyclotrisiloxane content probably originated from TIP and
385 TPMP (Fig. 3). Tetramethylsilane is used as a starting material for synthesizing more complex
386 organosilanes, and the tetramethylsilane detected in field measurement 2 might have also originated
387 from TIP and TPMP. In addition, propyl propionate is a safer substitute for toluene because of its low
388 odor, moderately volatile nature, and nonhazardous and nonpolluting ester product; thus, the propyl
389 propionate detected in field measurement 2 mainly originated from industrial emissions. Alkanes
390 were the dominant VOCs at various altitudes and sites in field measurement 2. Thus, concentrations
391 of the VOCs originating from vehicle exhaust might have been higher than those of the VOCs
392 originating from industrial exhaust, which is line with the results of field measurement 1. The order
393 of average VOC concentrations at the three sites in field measurement 2 was as follows: site 3 > site
394 1 > site 2. This order differed from that in field measurement 1, and this difference was probably
395 because the prevailing winds in the study area changed from north–northeast in field measurement 1
396 to northeast by east in field measurement 2.

397 **4 Discussion**

398 In this study, a UAV platform with sensing and sampling systems was developed for 3D air
399 pollutant concentration measurements. This platform was used in two measurement periods for



400 detecting air pollutant concentrations in a large special industrial zone that includes a traditional
401 industrial park, precision machinery park, and municipal waste incineration plant. To elucidate the
402 transport of air pollutants in the aforementioned industrial zone, this study used a single theodolite
403 on the ground to measure the speeds and directions of the upper winds during the field measurement
404 periods. The use of this method prevented the airflow caused by the rotor of the UAV from influencing
405 the measurements. The measurement results obtained by the sensing system of the developed
406 platform, which contains multiple microsensors and is integrated with IoT technology, demonstrated
407 the feasibility of this platform for determining the real-time 3D distributions of critical air pollutants.
408 The NO₂ and O₃ contents were 0 ppm in the two field measurements because the sensitivities of the
409 NO₂ and O₃ sensors were too low. All VOC concentrations at the three field measurement sites were
410 very low (≤ 0.02 ppm), possibly because the sensitivity of the VOC sensor was also too low. The sum
411 of the O₃ and NO₂ concentrations ($[O_3] + [NO_2]$) is defined as odd oxygen (ODO) in atmospheric
412 chemistry (Yee et al., 2021; Zhang et al., 2018). Many studies have indicated that a high positive
413 correlation exists between the concentrations of ODO and secondary organic aerosols (SOA's)
414 (Hernod et al., 2008; Wood et al., 2010; Hu et al., 2016); thus, the concentration of SOA can be
415 represented by the sum of the O₃ and NO₂ concentrations. SOA can have detrimental effects on the
416 health and mortality of patients with chronic inflammatory diseases (Déméautis et al., 2022).
417 Therefore, developing highly sensitive O₃, NO₂, and VOC microsensors is desirable for improving
418 UAV air pollutant telemetry.

419 The sampling system of the developed platform, which contains multiple remote-controllable
420 gas sampling sets, can conduct multipoint sampling according to the relevant situation for analyzing
421 the composition of air pollutants. The results show that it is feasible to replace a canister with the
422 sampling bag 1-L Tedlar bag for the 3D measurement of VOC concentrations according to the
423 procedures of the TO-15 method of the US EPA. Moreover, the three air pumps of the gas sampling
424 kits are connected in parallel to a length of 60-cm vertical sampling tube at the top of the UAV. The
425 dispersion effects of drone propellers are small in the monitoring of atmospheric pollutants (Fan et
426 al., 2023) but cause a large negative bias in the measurement of pollutant concentrations in plumes.
427 (Villa et al., 2016). Therefore, the arrangement of the vertical sampling pipe is acceptable.

428 The observation and analysis data obtained from the single-theodolite method, sensing system,
429 and sampling system were used to examine the effect of air pollutant discharge from the investigated
430 industrial zone on the study area. The results of this study indicate the feasibility of using the
431 developed UAV platform to accurately identify pollutants and determine their 3D spatial distributions
432 concentrations in a study area. Thus, the UAV platform can serve as a useful tool in the management
433 and decision-making process of air pollution in industrial areas.

434 5 Conclusions

435 Most research on the application of UAV systems in air pollution monitoring has focused on the
436 development of microsensors and control and communication systems; few studies have used UAV
437 systems for the sampling and analysis of pollutants at high altitudes. Therefore, in the present study,
438 a UAV platform with sensing and sampling systems was developed for 3D air pollutant concentration



439 measurements. The sensing system of this platform contains multiple microsensors and IoT
440 technologies for obtaining the real-time 3D distributions of critical air pollutants. The sampling
441 system contains multiple remote-controllable gas sampling sets as sampling devices, and these
442 sampling sets contain a 1-L Tedlar bag instead of a canister for the 3D measurement of VOC
443 concentrations in accordance with the TO-15 method of the US EPA. The developed platform was
444 used to detecting air pollutant emissions in a large special industrial zone that includes a traditional
445 industrial park, precision machinery park, and municipal waste incineration plant. According to the
446 local prevailing wind direction in the study area, three field measurement sites were selected—one
447 site located upwind and two sites located downwind. Comprehensive air pollutant characterization
448 was performed in the aforementioned industrial zone during two field measurements in March and
449 May 2023. The results of this characterization indicate that the developed UAV platform can
450 accurately obtain the 3D concentration distributions of critical air pollutants in real time and conduct
451 multipoint sampling according to the relevant situation for analyzing the composition of air pollutants.

452 *Data availability.* Data not available - participant consent.

453 *Author contributions.* CWL developed the concept and methodology for this work. CWL and CHS
454 processed the field measurements data collected, and analysis of the samples. CWL provided
455 scientific expertise on in situ data. Data handling and analysis were performed by CHS with
456 contributions from CWL. All authors contributed to the proofreading and added valuable suggestions
457 to the final draft.

458 *Competing interests.* The contact author has declared that none of the authors has any competing
459 interests.

460 *Acknowledgments.* The authors gratefully acknowledgments distinguished Professor Jeng-Jong
461 Liang, Feng Chia University, Taiwan, for providing the air pollution expertise and using his gas
462 chromatography/mass spectrometry; and like to thank Green Ideas Synergy Co., Taiwan, for
463 providing the micro sensors and using company's IoT framework for this research.

464 *Financial support.* This research has been supported by the Taichung City Environmental Protection
465 Bureau, Taiwan, for financially supporting this research under Taichung EPB-P1111017073.

466 **References**

- 467 Alvarado, M., Gonzalez, F., Fletcher, A., Doshi, A.: Towards the development of a low cost airborne
468 sensing system to monitor dust particles after blasting at open-pit mine sites. *Sensors* 15,
469 19667–19687, <https://doi.org/10.3390/s150819667>, 2015.
- 470 Arroyo, P., Gómez-Suárez, J., Herrero, J. L., Lozano, J.: Electrochemical gas sensing module
471 combined with Unmanned Aerial Vehicles for air quality monitoring. *Sens. Actuators B. Chem.*
472 364, 131815, <https://doi.org/10.1016/j.snb.2022.131815>, 2022.
- 473 Boursianis, A. D., Papadopoulou, M. S., P. Diamantoulakis, et al.: Internet of Things (IoT) and
474 Agricultural Unmanned Aerial Vehicles (UAVs) in smart farming: A comprehensive review.



- 475 Internet of Things 18, 100187, <https://doi.org/10.1016/j.iot.2020.100187>, 2022.
- 476 Cozma, A., Firculescu, A. C., Tudose, D., Ruse, L.: Autonomous multi-rotor aerial platform for air
477 pollution monitoring. *Sensors* 22(3), 860, <https://doi.org/10.3390/s22030860>, 2022.
- 478 De Fazio, R., Matteo Dinoi, L., De Vittorio, M., Visconti, P.: A sensor-based drone for pollutants
479 detection in Eco-Friendly Cities: Hardware design and data analysis application. *Electronics* 11,
480 52, <https://doi.org/10.3390/electronics11010052>, 2022.
- 481 Déméautis, T., Delles, M., Tomaz, S., Monneret, G., Glehen, O., Devouassoux, G., George, C.,
482 Bentaher, A.: Pathogenic mechanisms of secondary organic aerosols. *Chem. Res. Toxicol.* 35(7),
483 1146–1161, <https://doi.org/10.1021/acs.chemrestox.1c00353>, 2022.
- 484 Duangsuwan, S., Prapruetdee, P., Subongkod, M., Klubsuwan, K.: 3D AQI mapping data assessment
485 of low-altitude drone real-time air pollution monitoring. *Drones* 6, 191,
486 <https://doi.org/10.3390/drones6080191>, 2022.
- 487 Fan, G., Liu, Z., Qin, Y., Long, B., Li, H., Li, J.: Airflow characteristics of rotorcraft plant protection
488 UAV operating in rice fields. *Biosyst. Eng.* 226, 209–222,
489 <https://doi.org/10.1016/j.biosystemseng.2023.01.007>, 2023.
- 490 Galle, B., Arellano, S., Bobrowski, N., et. al.: A multi-purpose, multi-rotor drone system for long-
491 range and high-altitude volcanic gas plume measurements. *Atmos. Meas. Tech.* 14, 4255–4277,
492 <https://doi.org/10.5194/amt-14-4255-2021>, 2021.
- 493 Gu, Q., Jia, C.: A consumer UAV-based air quality monitoring system for smart cities. 2019 IEEE
494 International Conference on Consumer Electronics (ICCE), DOI: 10.1109/ICCE.2019.8662050,
495 2019.
- 496 Gu, Q., Michanowicz, D. R., Jia, C.: Developing a modular unmanned aerial vehicle (UAV) platform
497 for air pollution profiling. *Sensors* 18, 4363, <https://doi.org/10.3390/s18124363>, 2018.
- 498 Herndon, S. C., Onasch, T. B., Wood, E. C., Kroll, J. H., et al.: Correlation of secondary organic
499 aerosol with odd oxygen in Mexico City. *Geophys. Res. Lett.* 35, 15804,
500 doi:10.1029/2008GL034058, 2008.
- 501 Hu, W., Hu, M., Hu, W., Jimenez, J. L., Yuan, B., Chen, W., et al.: Chemical composition, sources,
502 and aging process of submicron aerosols in Beijing: Contrast between summer and winter. *J.*
503 *Geophys. Res. Atmos.* 121 (2016) 1955–1977, <https://doi.org/10.1002/2015JD024020>, 2016.
- 504 Huang, F., Peng, S., Yang, H., Cao, H., Ma, N., Ma, L.: Development of a novel and fast XRF
505 instrument for large area heavy metal detection integrated with UAV. *Environ. Res.* 214, 113841,
506 <https://doi.org/10.1016/j.envres.2022.113841>, 2022.
- 507 Liu, C., Huang, J., Wang, Y., Tao, X., Hu, C., Deng, L., Xu, J., Xiao, H. W., Luo, L., Xiao, H. Y., Xiao,
508 W.: Vertical distribution of PM_{2.5} and interactions with the atmospheric boundary layer during the
509 development stage of a heavy haze pollution event. *Sci. Total Environ.* 704, 135329,
510 <https://doi.org/10.1016/j.scitotenv.2019.135329>, 2020.
- 511 Middleton, W. E. K., Spilhaus A. F.: *Meteorological Instruments*. 3rd ed., Heritage: University of
512 Toronto Press. pp181-183. doi.org/10.3138/9781487572013-056, 2019.
- 513 Noori, R., Dahnil, D. P.: The effects of speed and altitude on wireless air pollution measurements



- 514 using hexacopter drone. (IJACSA) Int. J. Adv. Comput. Sci. Appl. 11(9), 268-276,
515 (DOI): 10.14569/IJACSA.2020.0110931, 2020.
- 516 Pochwała, S., Gardecki, A., Lewandowski, P., Somogyi, V., Anweiler, S.: Developing of low-cost air
517 pollution sensor—Measurements with the unmanned aerial vehicles in Poland. *Sensors* 20, 3582,
518 <https://doi.org/10.3390/s20123582>, 2020.
- 519 Qiu, S., Chen, B., Wang, R., Zhu, Z., Wang, Y., Qiu, X.: Estimating contaminant source in chemical
520 industry park using UAV-based monitoring platform, artificial neural network and atmospheric
521 dispersion simulation. *RSC Adv.* 7, 39726–39738, <https://doi.org/10.1039/C7RA05637K>, 2017.
- 522 Samad, A., Florez, D.A., Chourdakis, I., Vogt, U.: Concept of using an unmanned aerial vehicle (UAV)
523 for 3D investigation of air quality in the atmosphere—Example of measurements near a roadside.
524 *Atmosphere* 13, 663, <https://doi.org/10.3390/atmos13050663>, 2022.
- 525 Shen, L., Cheng, Y., Bai, X., Dai, H., et al.: Vertical profile of aerosol number size distribution during
526 a haze pollution episode in Hefei, China. *Sci. Total Environ.* 814, 152693,
527 <https://doi.org/10.1016/j.scitotenv.2021.152693>, 2022.
- 528 Singh, P. K., Sharma, A.: An intelligent WSN-UAV-based IoT framework for precision agriculture
529 application. *Comput. Electr. Eng.* 100, 107912,
530 <https://doi.org/10.1016/j.compeleceng.2022.107912>. 2022.
- 531 Sun, X., Zhao, T., Tang, G., Bai, Y., et al.: Vertical changes of PM_{2.5} driven by meteorology in the
532 atmospheric boundary layer during a heavy air pollution event in central China. *Sci. Total Environ.*
533 858, 159830, <https://doi.org/10.1016/j.scitotenv.2022.159830>, 2023.
- 534 Suroto, A., Ubaidillah, A., Ulum, M.: Air condition monitoring using way point based UAV
535 (Unmanned Aerial Vehicle). *Int. J. Sci. Eng. Inf. Technol.* 3(1), 109–114,
536 <https://journal.trunojoyo.ac.id/ijseit>, 2018.
- 537 Villa, T. F., Salimi, F., Morton, K., Morawska, L., Gonzalez, F.: Development and validation of a
538 UAV based system for air pollution measurements. *Sensors* 16, 2202,
539 <https://doi.org/10.3390/s16122202>, 2016.
- 540 Wood, E. C., Canagaratna, M. R., Herndon, S. C., et al.: Investigation of the correlation between odd
541 oxygen and secondary organic aerosol in Mexico City and Houston. *Atmos. Chem. Phys. Discuss.*
542 10 (2010) 8947–8968, <https://doi.org/10.5194/acp-10-8947-2010>, 2010.
- 543 Xie, T., Liu, R., Hai, R. T., Hu, Q. H., Lu. Q.: UAV platform based atmospheric environmental
544 emergency monitoring system design. *J. Appl. Sci.* 13(8), 1289–1296,
545 DOI: 10.3923/jas.2013.1289.1296, 2013.
- 546 Yang, Z., Yu, X., Dedman, S., Rosso, M., Zhu, J., Yang, J., Xia, Y., Tian, Y., Zhang, G., Wang, J.:
547 UAV remote sensing applications in marine monitoring: Knowledge visualization and review. *Sci.*
548 *Total Environ.* 838, 155939, <https://doi.org/10.1016/j.scitotenv.2022.155939>, 2022.
- 549 Yee, L. D., Craven, J. S., Loza, C. L., Schilling, K. A., Ng, N. L., et al.: Secondary organic aerosol
550 formation from low-NO_x photooxidation of dodecane: evolution of multigeneration gas-phase
551 chemistry and aerosol composition, *J. Phys. Chem. A* 116(24), 6211–6230,
552 <https://doi.org/10.1021/jp211531h>, 2021.



- 553 Yee, L., Pollak, W., Brunt, D., et al.: A new theodolite for following fast moving objects especially
554 for making pilot balloon observations of greater accuracy. *Q. J. R. Meteorol. Soc.* 65, 443–447,
555 <https://doi.org/10.1002/qj.49706528117>, 1939.
- 556 Yungaicela-Naula, N. M., Garza-Castañón, L. E., Mendoza-Domínguez, A., Minchala-Avila, L. I.,
557 Garza-Elizondo, L. E.: Design and implementation of an UAV-based platform for air pollution
558 monitoring and source identification. 2017 Congreso Nacional de Control Automático, Monterrey,
559 Nuevo León, Mexico. <https://amca.mx/memorias/amca2017/media/files/0041.pdf>, 2017.
- 560 Zhang, C., Lu, X. H., Zhai, J. H., Chen, H., Yang, X., Zhang, Q., et al.: Insights into the formation of
561 secondary organic carbon in the summertime in urban Shanghai. *J Environ Sci -China*. 72, 118–
562 132, <https://doi.org/10.1016/j.jes.2017.12.018>, 2018.
- 563 Zheng, T., Li, B., Li, X. B., Wang, Z., Li, S. Y., Peng, Z. R.: Vertical and horizontal distributions of
564 traffic-related pollutants beside an urban arterial road based on unmanned aerial vehicle
565 observations. *Build. Environ.* 187, 107401, <https://doi.org/10.1016/j.buildenv.2020.107401>, 2021.
566